

ORIGINAL RESEARCH



## Landscape of infiltrating B cells and their clinical significance in human hepatocellular carcinoma

Zhao Zhang<sup>a,b\*</sup>, Lijie Ma<sup>a\*</sup>, Shyamal Goswami<sup>b\*</sup>, Jiaqiang Ma<sup>b</sup>, Bohao Zheng<sup>a</sup>, Meng Duan<sup>a</sup>, Longzi Liu<sup>a</sup>, Lijun Zhang<sup>c</sup>, Jiyei Shi<sup>a</sup>, Liangqing Dong<sup>a</sup>, Yumeng Sun<sup>b</sup>, Lingyu Tian<sup>a</sup>, Qiang Gao<sup>a,d</sup>, and Xiaoming Zhang<sup>b</sup>

<sup>a</sup>Department of Liver Surgery and Transplantation, Liver Cancer Institute, Zhongshan Hospital, Fudan University; Key Laboratory of Carcinogenesis and Cancer Invasion of Ministry of Education, Shanghai, China; <sup>b</sup>Key Laboratory of Molecular Virology & Immunology, Institut Pasteur of Shanghai, Chinese Academy of Sciences, Shanghai, China; <sup>c</sup>Department of Electrical and System Engineering, Washington University in St. Louis, St. Louis, MO, USA; <sup>d</sup>State Key Laboratory of Genetic Engineering, Fudan University, Shanghai, China

### ABSTRACT

As a major cellular component in tumor microenvironment, the distribution, frequency, and prognostic significance of infiltrating B cell subsets in hepatocellular carcinoma (HCC) remain controversial. Using tyramide signal amplification (TSA) based fluorescent multiplexed immunohistochemistry *in situ*, we evaluated the distribution and frequency of B cell subsets in two independent HCC cohorts (n = 619). The results were further confirmed by flow cytometry. Correlations of B cell subsets with clinicopathologic features and patient prognosis were analyzed. Five B cell subsets were defined by multiplexed immunohistochemistry and each subset was clearly separated by t-SNE dimension reduction analysis. Notably, the densities of all B cell subsets were significantly decreased in the tumor. The frequency of plasma cells within B cells was most abundant in the tumor. In training cohort (n = 258), high densities of tumor-infiltrating CD20<sup>+</sup> B cells, naive B cells, IgM<sup>+</sup> memory B cells, CD27<sup>-</sup> isotype-switched memory B cells, and plasma cells were associated with superior survival. Multivariate analysis further identified CD20<sup>+</sup> B cells, naive B cells, and CD27<sup>-</sup> isotype-switched memory B cells as independent prognosticators for survival. Unsupervised cluster analysis confirmed increased B cell subsets harbored superior survival. In addition, high density of B cells was correlated with smaller tumor size and well differentiation. The results were validated in the independent cohort of 361 HCC patients. Intratumor infiltration of B cells is significantly impaired during HCC progression. High densities of tumor-infiltrating B cells imply a better clinical outcome. Therapies designed to target B cells may be a novel strategy in HCC.

### ARTICLE HISTORY

Received 29 September 2018  
Revised 24 December 2018  
Accepted 3 January 2019

### KEYWORDS

Liver cancer; tumor microenvironment (TME); B cell subsets; tyramide signal amplification (TSA); prognosis





### Introduction

Hepatocellular carcinoma (HCC) is one of the leading causes of cancer-related death worldwide, with limited treatment options and high mortality rate.<sup>1</sup> Various risk factors for HCC are well defined, such as hepatitis virus infection, alcohol consumption, and metabolic syndrome. These risk factors ultimately result in an inflamed fibrotic or cirrhotic liver with extensive immune infiltration which is regarded as a key contributor to hepatocarcinogenesis and tumor progression.<sup>2,3</sup> Recent breakthrough of nivolumab (anti-PD-1 Ab) reaching a response rate of 15–20% in advanced HCC patients has sparked great interest in HCC immunotherapy.<sup>4</sup> Further understanding of immune components within HCC will help to identify new immunotherapeutic targets.

The immune microenvironment in HCC is a mixture of heterogeneous immune components.<sup>5</sup> T cells are always the hot spots in the antitumor activity of HCC. A recent study has identified eleven T cell subsets in HCC based on their molecular features derived from large-scale single-cell transcriptome


sequencing.<sup>6</sup> Meanwhile, the optimized curative effects of chimeric antigen receptor T-cell immunotherapy in solid tumor inspired the investigation of CD8<sup>+</sup> T cells in HCC.<sup>7</sup> In addition, macrophages, neutrophils, natural killer cells, and natural killer T cells have also been extensively investigated in HCC, either promoting or alternatively inhibiting antitumor immunity.<sup>5</sup> These findings highlighted HCC as an immunogenic tumor and provided the rationale for immunomodulatory approaches as alternative treatment strategies. However, as a critical player in humoral immune response, the clinical relevance and prognostic significance of B cells and their subsets in HCC were poorly defined.

B cells consistently represent a substantial cellular component in tumor microenvironment, who exert their functions through antibody production, antigen presentation, and immune regulation.<sup>8,9</sup> Some investigations have indicated that tumor-infiltrating B cells were associated with favorable prognosis in human solid tumors, such as breast cancer,<sup>10</sup> oral cancer,<sup>11</sup> non-

**CONTACT** Qiang Gao  [gaoqiang@fudan.edu.cn](mailto:gaoqiang@fudan.edu.cn)  Department of Liver Surgery and Transplantation, Liver Cancer Institute, Zhongshan Hospital, Fudan University, 180 Fenglin Road, Shanghai 200032, China; Xiaoming Zhang  [xmzhang@ips.ac.cn](mailto:xmzhang@ips.ac.cn)  Key Laboratory of Molecular Virology & Immunology, Institut Pasteur of Shanghai, Chinese Academy of Sciences, Shanghai 200032, China

\*These authors contributed equally to this work.

Color versions of one or more of the figures in the article can be found online at [www.tandfonline.com/koni](http://www.tandfonline.com/koni).

 Supplemental data for this article can be accessed on the publisher's website.

small cell lung cancer (NSCLC),<sup>12,13</sup> ovarian cancer,<sup>14</sup> and melanoma.<sup>15</sup> The underlying mechanisms include inducing tumor cell apoptosis through antibody-dependent cell-mediated cytotoxicity and serving as an antigen presenting cells to activate effector cells.<sup>16,17</sup> By contrast, several studies also argued that B cells could possess a suppressive function to promote tumor progression and inhibit antitumor immunity in lung cancer,<sup>18</sup> prostate cancer,<sup>19,20</sup> melanoma,<sup>21,22</sup> and pancreatic cancer.<sup>23,24</sup> This complex situation also happens in HCC. We have previously reported a population of atypical memory B cells that possessed tumor-killing potential and indicated a favorable prognosis within HCC microenvironment,<sup>25</sup> while others argued that PD-1<sup>hi</sup> or CXCR3<sup>+</sup> B cells promoted HCC progression.<sup>26,27</sup> Human B cells can be divided into several subsets based on different developmental stages, including naive B cells (Bn), IgM<sup>+</sup> memory B cells (IgM<sup>+</sup> Bm), CD27<sup>+</sup> isotype-switched memory B cells (CD27<sup>+</sup> Sw Bm), CD27<sup>-</sup> isotype-switched memory B cells (CD27<sup>-</sup> Sw Bm), and terminally differentiated plasma cells (PCs). Generally, under the action of cytokines including IL-10 and IL-21, Bn can undergo isotype switching, PC generation, and Ab secretion.<sup>28</sup> IgM<sup>+</sup> Bm and Sw Bm could differentiate rapidly into PCs.<sup>29</sup> However, few studies have detailed the subsets of B cells in human normal or neoplastic tissues, particularly with *in situ* techniques.

To provide a comprehensive view of tumor-infiltrating B cells in HCC, fluorescent multiplexed immunohistochemistry was used to determine the subset, density, and distribution of B cells in tumor tissues and paired non-tumor liver tissues. Furthermore, flow cytometry analysis was used to validate the immunohistochemistry results. We found that high densities of certain B cell subsets or B cell clusters indicated a significantly prolonged survival in HCC. These findings suggest that B cell subsets might represent a target for immunotherapy and open up new avenues for future research of tumor-infiltrating B cells in HCC.

## Results

### Multiplexed sequential immunohistochemistry enabling definition of B cell subsets in HCC

To *in situ* characterize resident and infiltrating B cell landscape in HCC, we established and optimized a multiplexing sequential immunohistochemistry workflow (Supplementary Figures S1A and S1B), encompassing five distinct markers to exhibit B cell subsets simultaneously. After spectral unmixing using inForm software, raw images were separated to its intrinsic fluorophores and the corresponding original 3,3'-diaminobenzidine (DAB) images were visualized (Figure 1a). The markers used to define five B cell subsets in this study were shown in Figure 1b. All markers were located on the cytoplasm of DAPI labeled immune cells in tumor tissues and non-tumor liver tissues which could be distinctly separated with visual sight (Figure 1c). Therefore, this method enabled us to identify and quantify five distinct B cell subsets by combined staining of CD20, CD24, CD27, CD38, IgM, and DAPI (Figure 1d, Supplementary Figures S1C and S1D).

### Multiparameter method enabling specific assessment of B cell subsets in multiplexed immunohistochemistry

In order to enable a specific assessment of B cell subsets, we generated a multiparameter method via evaluation of single cell fluorescent pixel intensity. Special gating strategies were developed to present five distinct B cell subsets in tumor and non-tumor liver tissues by using the software of FCS Express (Figure 2a and b). In a representative sample, a higher proportion of CD20<sup>+</sup> B cells was observed in non-tumor liver tissues (4.58%) compared to tumor tissues (2.35%). Based on positive expression of CD20, cells could be classified into CD27-positive (tumor: 45.21%, non-tumor liver: 35.44%) and CD27-negative (tumor: 45.14%, non-tumor liver: 62.63%). Meanwhile, IgM was combined to separate CD20<sup>+</sup>CD27<sup>+</sup> cells (tumor: IgM<sup>-</sup> 59.17%, IgM<sup>+</sup> 37.18%; non-tumor liver: IgM<sup>-</sup> 64.14%, IgM<sup>+</sup> 31.55%, respectively) and CD20<sup>+</sup>CD27<sup>-</sup> cells (tumor: IgM<sup>-</sup> 46.08%, IgM<sup>+</sup> 49.34%; non-tumor liver: IgM<sup>-</sup> 57.01%, IgM<sup>+</sup> 37.78%, respectively). Thus, CD20<sup>+</sup> B cells were classified into four subsets: Bn (CD20<sup>+</sup>CD27<sup>-</sup>IgM<sup>+</sup>), IgM<sup>+</sup> Bm (CD20<sup>+</sup>CD27<sup>+</sup>IgM<sup>+</sup>), CD27<sup>-</sup> Sw Bm (CD20<sup>+</sup>CD27<sup>-</sup>IgM<sup>-</sup>) and CD27<sup>+</sup> Sw Bm (CD20<sup>+</sup>CD27<sup>+</sup>IgM<sup>-</sup>). Meanwhile, PCs were defined as CD20<sup>-</sup>CD24<sup>-</sup>CD27<sup>hi</sup>CD38<sup>hi</sup> (Figure 2a and b). In addition, we revealed the distinct classification of these five B cell subsets with t-SNE by dimension reduction analysis (Figure 2c). These five distinct B cell subsets could be separated independently in tumor and non-tumor liver. Moreover, Bn might be further divided into two subsets in accordance with their distribution on the dimension reduction analysis. These findings indicated that the method of multiplexed immunohistochemistry could accurately classify B cell subsets in liver tissues with well-established differentiation markers.

### Distribution of B cell subsets in HCC

In the training cohort, a significantly higher density of CD20<sup>+</sup> B cell infiltration was found in non-tumor liver tissues (median, 619 cells/mm<sup>2</sup>) than tumor tissues (median, 160 cells/mm<sup>2</sup>,  $P < 0.001$ ). Analogously, higher infiltration of PCs was noted in non-tumor liver tissues (median, 426 cells/mm<sup>2</sup>) than tumor tissues (median, 286 cells/mm<sup>2</sup>,  $P = 0.044$ ) (Figure 2d). Among CD20<sup>+</sup> B cells, we focused on four specific subsets including Bn, IgM<sup>+</sup> Bm, CD27<sup>-</sup> Sw Bm, and CD27<sup>+</sup> Sw Bm. Significantly more Bn cells were detected in non-tumor liver tissues (median, 154 cells/mm<sup>2</sup>) compared to tumor tissues (median, 36 cells/mm<sup>2</sup>,  $P < 0.001$ ). Similarly, a higher density of IgM<sup>+</sup> Bm cells was also found in non-tumor liver tissues (median, 71 cells/mm<sup>2</sup>) than those in tumor tissues (median, 33 cells/mm<sup>2</sup>,  $P < 0.001$ ). In addition, non-tumor liver tissues harbored increased counts of both CD27<sup>+</sup> Sw Bm (median, 266 cells/mm<sup>2</sup>) and CD27<sup>-</sup> Sw Bm (median, 128 cells/mm<sup>2</sup>) compared to tumor tissues (CD27<sup>+</sup> Sw Bm, median, 28 cells/mm<sup>2</sup>,  $P < 0.001$ ; CD27<sup>-</sup> Sw Bm, median, 63 cells/mm<sup>2</sup>,  $P < 0.001$ ). Similar distribution status was observed in the validation cohort (Figure 2d). Additionally, the numbers of B cell subsets showed a positive correlation with each other (range of correlation coefficients, 0.37–0.65,  $P < 0.001$ ), which was also revealed

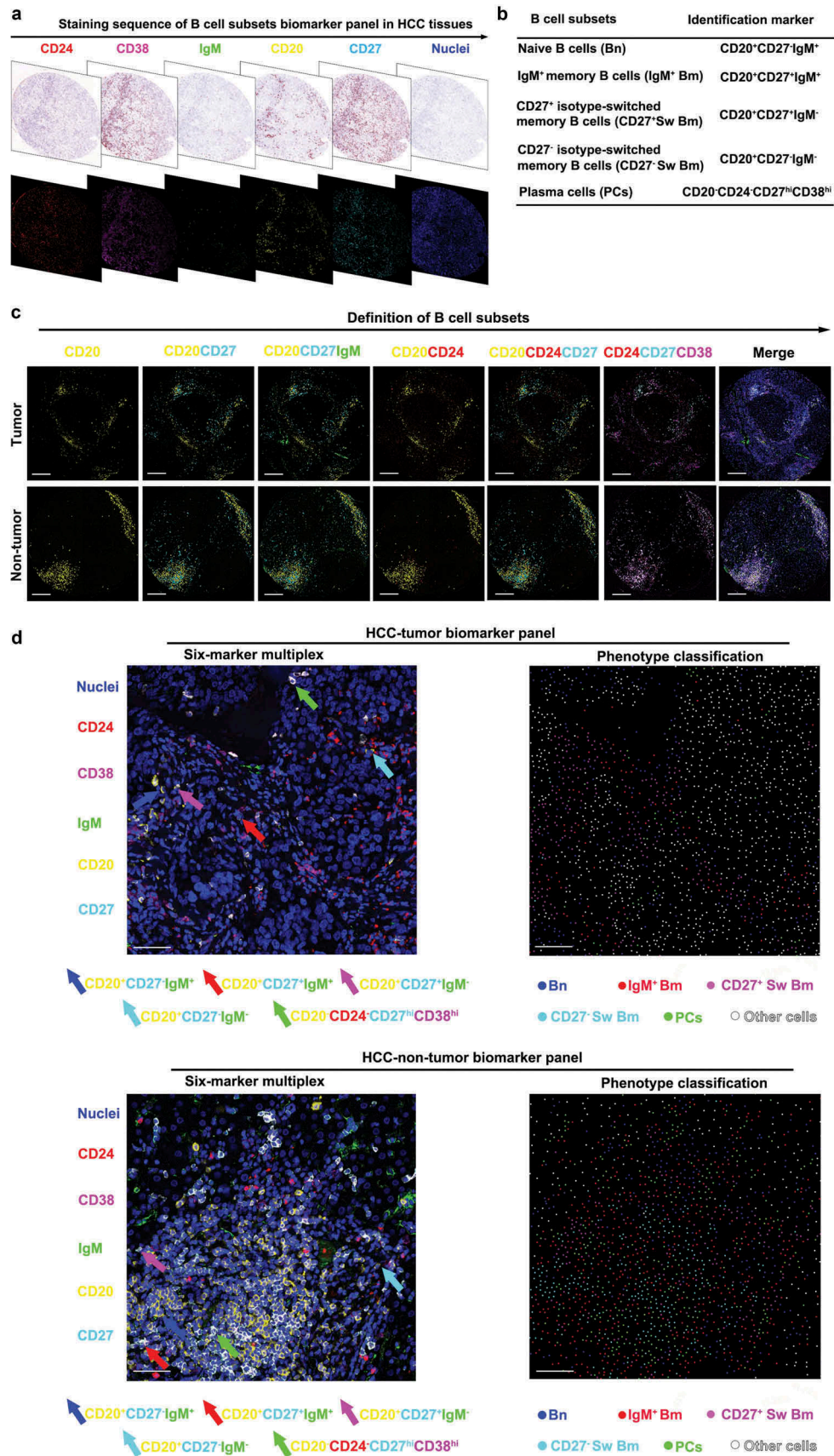


**Figure 1.** B cell subsets are defined by six-color multiplexed immunohistochemistry in HCC. (a) Digital scanning displayed bright-field image and multispectral image (MSI) of one TMA core from HCC tissues. (b) B cell subsets and corresponding identification markers applied in this study. (c) The multiplexed images displayed co-localization of different markers. Scale bar: 200  $\mu$ m. (d) The representative images of six-marker multiplex and phenotype classification. Scale bar: 50  $\mu$ m.



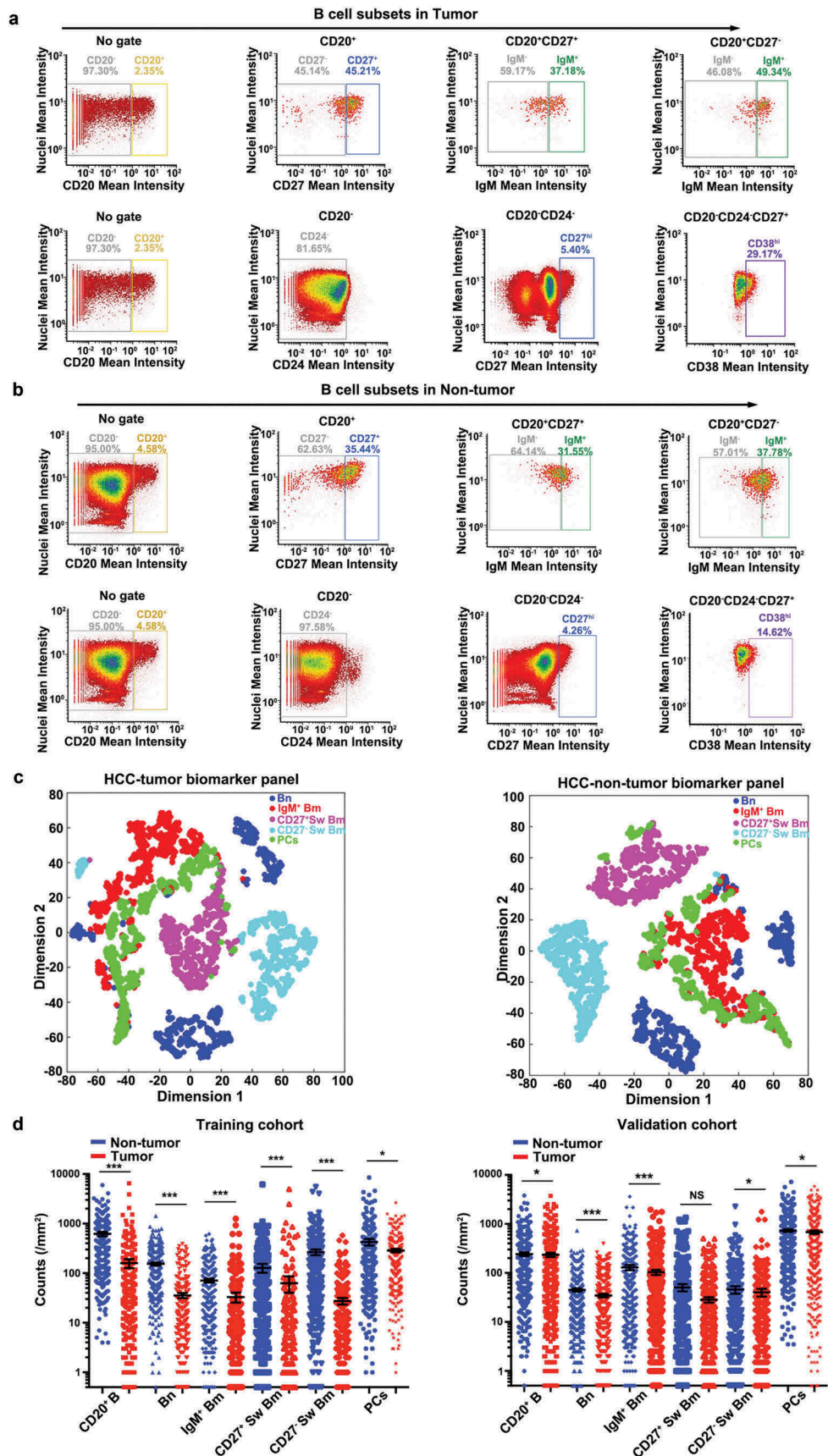


**Figure 2.** B cell subset distributions are compared between tumor and non-tumor liver tissues of HCC. (a and b) The acquired single-cell fluorescent pixel intensity data were visualized and analyzed by FCS Express 6 Plus v6.04.0034 (De Novo Software). Five distinct B cell subsets were gated, and represented as image plots of tumor (a) and non-tumor liver tissues (b). (c) The t-SNE analysis of B cells from tumor tissues and non-tumor liver tissues displayed the distinct classification of five distinct B cell subsets. (d) Comparisons of the B cell subset densities between tumor and non-tumor liver tissues in two independent cohorts. Statistical differences were determined by two-tailed student's *t* test. NS: not significant, \**P* < 0.05, \*\*\**P* < 0.001.

in the validation cohort (Table 1). Collectively, these results indicated that B cells were relatively abundant in normal liver tissues, while HCC encountered the change of B cell compartments in a global way, by decreasing all B cell subsets.

### Classification of B cell subsets in HCC by flow cytometry

To further explore the classification of B cells in HCC, we applied flow cytometry on tumor tissues, paired non-tumor liver tissues and PBMCs from 10 HCC patients (Figure 3a,

**Table 1.** Correlation among tumor-infiltrating B subsets (n = 619).

| Variable                           | PCs  |        | CD27 <sup>+</sup> Sw Bm |        | CD27 <sup>-</sup> Sw Bm |        | Bn   |        |
|------------------------------------|------|--------|-------------------------|--------|-------------------------|--------|------|--------|
|                                    | r    | P      | r                       | P      | r                       | P      | r    | P      |
| <b>Training cohort (n = 258)</b>   |      |        |                         |        |                         |        |      |        |
| IgM <sup>+</sup> Bm                | 0.52 | <0.001 | 0.51                    | <0.001 | 0.61                    | <0.001 | 0.65 | <0.001 |
| Bn                                 | 0.37 | <0.001 | 0.52                    | <0.001 | 0.45                    | <0.001 |      |        |
| CD27 <sup>-</sup> Sw Bm            | 0.50 | <0.001 | 0.63                    | <0.001 |                         |        |      |        |
| CD27 <sup>+</sup> Sw Bm            | 0.41 | <0.001 |                         |        |                         |        |      |        |
| CD20 <sup>+</sup> B                | 0.48 | <0.001 |                         |        |                         |        |      |        |
| <b>Validation cohort (n = 361)</b> |      |        |                         |        |                         |        |      |        |
| IgM <sup>+</sup> Bm                | 0.66 | <0.001 | 0.39                    | 0.047  | 0.49                    | <0.001 | 0.66 | <0.001 |
| Bn                                 | 0.50 | <0.001 | 0.53                    | <0.001 | 0.50                    | <0.001 |      |        |
| CD27 <sup>-</sup> Sw Bm            | 0.40 | <0.001 | 0.60                    | <0.001 |                         |        |      |        |
| CD27 <sup>+</sup> Sw Bm            | 0.21 | <0.001 |                         |        |                         |        |      |        |
| CD20 <sup>+</sup> B                | 0.52 | <0.001 |                         |        |                         |        |      |        |

**Abbreviation:** CD20<sup>+</sup> B, CD20<sup>+</sup> B cells; IgM<sup>+</sup> Bm, IgM<sup>+</sup> memory B cells; Bn, naïve B cells; CD27<sup>-</sup> Sw Bm, CD27<sup>-</sup> isotype-switched memory B cells; CD27<sup>+</sup> Sw Bm, CD27<sup>+</sup> isotype-switched memory B cells; PCs, plasma cells. Pearson's correlation test.

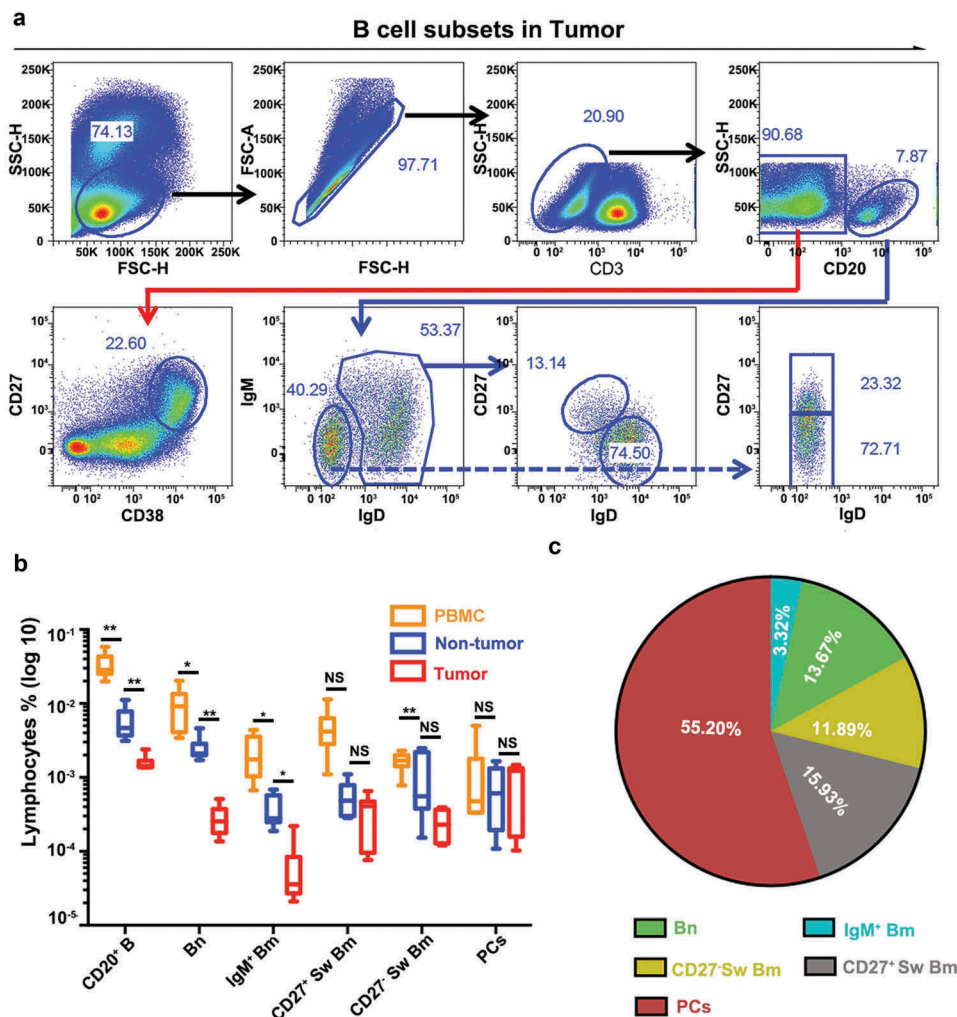


**Figure 3.** Flow cytometry confirms the classification of B cell subsets in HCC. (a) The gating strategy of five distinct B cell subsets in HCC tumor tissues by flow cytometry. (b) Comparisons of the frequencies of five B cell subsets among tumor tissues, non-tumor liver tissues and PBMCs (n = 10). NS: not significant, \*P < 0.05, \*\*P < 0.01. (c) The proportions of different subsets among B cell compartment (CD20<sup>+</sup> B cells plus PCs) were analyzed in tumor tissues.

Supplementary Figures S2A and S2B). Then, we compared the proportion of each B cell subset within total lymphocytes. CD20<sup>+</sup> B cell frequencies were significantly higher in the PBMC (3.24%), but were much lower in the non-tumor tissues (0.47%, PBMC versus non-tumor,  $P = 0.003$ ) or tumor tissues (0.093%, non-tumor versus tumor,  $P = 0.008$ ). Moreover, the flow cytometry analysis confirmed that significantly higher abundance of infiltrating Bn and IgM<sup>+</sup> Bm was detected in non-tumor liver tissues (Bn, 0.26%; IgM<sup>+</sup> Bm, 0.039%) compared to tumor tissues (Bn, 0.028%,  $P = 0.003$ ; IgM<sup>+</sup> Bm, 0.0069%,  $P = 0.016$ ) (Figure 3b). Frequencies of CD27<sup>+</sup> Sw Bm and CD27<sup>-</sup> Sw Bm within tumor tissues also had a decreased tendency toward statistical significance compared to those in non-tumor liver tissues. In addition, as the whole B cell compartment (CD20<sup>+</sup> B cells and PCs) were taken into account, we detected remarkable differences in the proportions of B cell subsets from different sources (Figure 3c, Supplementary Figures S2C and S2D). In tumor tissues, PCs (55.20%) constituted the highest proportion among all B cells and the proportions of other B cell subsets were 15.93% (CD27<sup>+</sup> Sw Bm), 13.67% (Bn), 11.89% (CD27<sup>-</sup> Sw Bm), and 3.32% (IgM<sup>+</sup> Bm), respectively (Figure 3c). However, in paired non-tumor liver tissues, Bn (47.09%) comprised the most abundant subset among B cell compartment and the proportions of other B cell subsets were 21.13% (CD27<sup>-</sup> Sw Bm), 14.04% (PCs), 10.52% (CD27<sup>+</sup> Sw Bm) and 7.22% (IgM<sup>+</sup> Bm), respectively (Supplementary Figure S2D).

As for the B cell subset proportions calculated by the immunohistochemistry data, in the training cohort, PCs (72.70%) were the most abundant cell type in tumor tissues and the proportions of other B cells were 10.75% (CD27<sup>-</sup> Sw Bm), 6.14% (Bn), 5.63% (IgM<sup>+</sup> Bm), and 4.78% (CD27<sup>+</sup> Sw Bm) respectively. In the non-tumor liver tissues, PCs occupied 31.60% and CD27<sup>+</sup> Sw Bm took up 29.39% of the total B cells, followed by Bn (17.02%), CD27<sup>-</sup> Sw Bm (14.14%), and IgM<sup>+</sup> Bm (7.85%), respectively (Supplementary Figure S2E). Similar results were found in the validation cohort (Supplementary Figure S2E). These results demonstrated a dynamic change of B cell subsets between tumor and non-tumor liver tissues. In particular, the proportion of PCs within B cells was most abundant in tumor tissues compared to non-tumor liver tissues, implying that an ongoing B cell response is happening in tumor microenvironment.

### Prognostic significance of tumor-infiltrating B cell subsets

We next investigated the correlations between tumor-infiltrating B cell subsets and patients' outcome. Surprisingly, except for CD27<sup>+</sup> Sw Bm cells, high infiltration of the remaining four B cell subsets significantly correlated with prolonged survival (OS, CD20<sup>+</sup> B, 63 versus 41 months,  $P = 0.036$ ; Bn, 63 versus 43 months,  $P = 0.022$ ; IgM<sup>+</sup> Bm, 63 versus 43 months,  $P = 0.023$ ; CD27<sup>-</sup> Sw Bm, 63 versus 43 months,  $P = 0.039$ ; CD27<sup>+</sup> Sw Bm, 62 versus 43 months,  $P = 0.080$ ; PCs, 62 versus 40 months,  $P = 0.016$ ) (Figure 4a). In the validation cohort, high densities of CD20<sup>+</sup> B cells, Bn

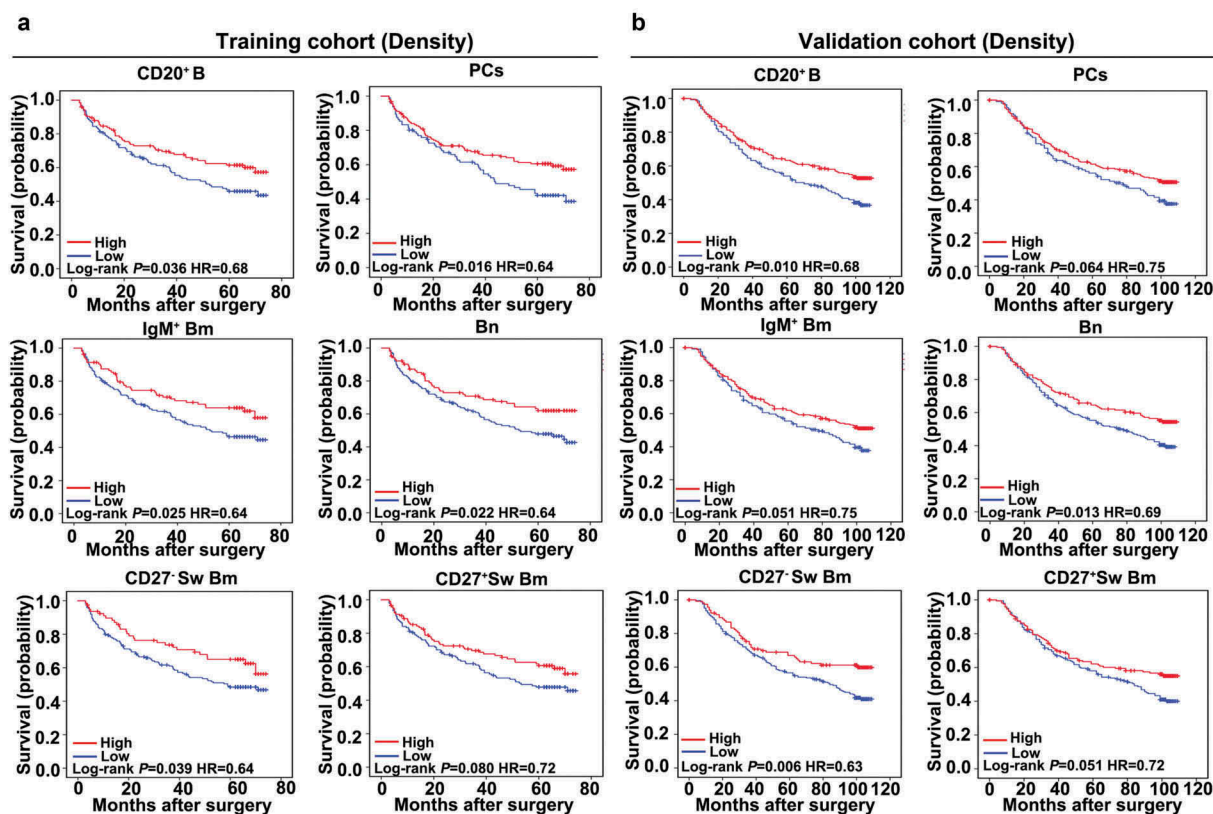


**Figure 4.** Tumor-infiltrating B cells significantly predict patient survival. (a and b) Kaplan-Meier analysis of OS for tumor-infiltrating B cell subsets based on cell density in the training and validation cohorts.



and CD27<sup>-</sup> Sw Bm also correlated with better OS (CD20<sup>+</sup> B, 84 versus 63 months,  $P = 0.010$ ; Bn, 93 versus 64 months,  $P = 0.013$ ; CD27<sup>-</sup> Sw Bm, 82 versus 75 months,  $P = 0.006$ ) (Supplementary Table S1; Figure 4b).

To extend the above findings, we evaluated the association between the expression of six B cell-related genes and HCC patient survival by using the TCGA (Cancer Genome Atlas) database. Interestingly, high expressions of these six B cell related genes were associated with improved survival in HCC (OS, CD79a,  $P = 0.002$ ; CD79b,  $P = 0.049$ ; MS4A (CD20),  $P = 0.002$ ; PAX5,  $P = 0.033$ ; IRF4,  $P = 0.023$ ; SLAMF7,  $P = 0.025$ ) (Supplementary Figure S3). So both our study and the TCGA data support a favorable outcome for those patients with a high infiltration of B cells.

### Association of tumor-infiltrating B cell subsets with clinicopathologic features

Next, we analyzed the correlation of densities of B cell subsets with clinicopathologic features. In the training cohort (Supplementary Table S4), high density of B cell and their subsets were associated with smaller tumor size ( $\leq 5$  cm) (CD20<sup>+</sup> B,  $P = 0.004$ ; Bn,  $P = 0.012$ ; IgM<sup>+</sup> Bm,  $P = 0.003$ ; CD27<sup>-</sup> Sw Bm,  $P = 0.001$ ; CD27<sup>+</sup> Sw Bm,  $P < 0.001$ ; PCs,  $P < 0.001$ . Meanwhile, high densities of CD20<sup>+</sup> B, CD27<sup>-</sup> Sw Bm, and CD27<sup>+</sup> Sw Bm as well as PCs were found to be associated with good differentiation (CD20<sup>+</sup> B,  $P = 0.008$ ; CD27<sup>-</sup> Sw Bm,  $P = 0.004$ ; CD27<sup>+</sup> Sw Bm,  $P = 0.002$ ; PCs,  $P = 0.015$ ). Similar results were also obtained in the validation cohort (Supplementary Table S5). These findings indicated that patients with high density of B cells harbored less aggressive clinicopathologic features.

### Clustering analysis affirming favorable prognostic value of B cells in HCC

Finally, we performed an unsupervised cluster analysis to integrate the densities of each B cell subset. Two different groups were revealed, in which the high-status group was characterized by increased infiltration of all five B cell subsets and the low-status group with a reduction of all five B cell subsets (Figure 5a and b). The high-status group harbored superior OS to the low-status group in both cohorts (training cohort, 63 versus 44 months,  $P = 0.021$ ; validation cohort, 89 versus 65 months,  $P = 0.018$ ) (Figure 5c). In multivariate analysis, the high-status group was an independent prognostic factor for OS (training cohort: HR = 0.60, 95%CI = 0.38–0.94,  $P = 0.026$ ; validation cohort: HR = 0.68, 95%CI = 0.50–0.92,  $P = 0.012$ ) (Supplementary Table S6). The results were in line with the above findings that high infiltration of B cell subsets indicated a better survival. Thus, the data further supported the hypothesis that B cells could potentially enhance the anti-tumor effect in HCC.

## Discussion

Herein, we identified five distinct B cell subsets at different developmental stages within tumor and non-tumor liver tissues using multiplexed immunostaining. In addition to the

highly distinct B cell profiles between HCC and non-tumor liver, we found that high densities of tumor-infiltrating B cells, Bn and CD27<sup>-</sup> Sw Bm were significantly and independently associated with better survival. These findings revealed the subset, distribution, and prognostic significance of infiltrating B cells in HCC patients, suggesting B cells' antitumor potential in HCC microenvironment.

As the key component of humoral immunity, the prognostic impacts of B cells in human solid tumor remain controversial. Previously, we have reported that increased CD20<sup>+</sup> B cells in tumor margin area correlated with favorable prognosis in HBV-associated HCC.<sup>25</sup> By contrast, a recent study reported high infiltration of CD20<sup>+</sup> B cells correlated poor survival in HCC.<sup>30</sup> Here, we further applied a panel of six markers in multiplexed immunochemistry to define five distinct B cell subpopulations. Of note, positively stained cells were measured by a unique automatic analysis and quantified by Vectra system other than manual calculation. We found that all B cell subsets were decreased in tumor compared to non-tumor liver tissues. Importantly, two out of the five B cell subsets (Bn and CD27<sup>-</sup> Sw Bm), as well as high-status of B cells based on cluster analysis of the five subsets, significantly and independently correlated with superior survival. Thus, our results again supported the notion that B cells generally exert an antitumor effect in human HCC.

In addition to the antitumor activities, tumor-infiltrating B cells could also dampen anti-tumor response via several possible ways. The differential roles of B cells in the tumor could be ascribed to their diverse subsets and functions in the tumor microenvironment. Our previous study described that CD20<sup>+</sup>IgD<sup>-</sup>IgM<sup>-/low</sup>IgG<sup>+</sup> B cells may enhance antitumor immunity by secreting IFN- $\gamma$  in HCC.<sup>25</sup> However, others have reported that PD1<sup>hi</sup>CD5<sup>hi</sup>CD24<sup>-/+</sup>CD27<sup>hi/+</sup> CD38<sup>dim</sup> B cells,<sup>26</sup> and CD20<sup>+</sup>FcyRII<sup>low/-</sup> B cells<sup>31</sup> could produce IL-10 to suppress the antitumor activity of cytotoxic T cells. Meanwhile, CD79a<sup>+</sup>CXCR3<sup>+</sup> B subset could induce the M2 macrophage polarization to accelerate tumorigenesis.<sup>27</sup> Therefore, B cells seemed to be highly heterogeneous, with multiple subsets co-existed within the tumor microenvironment. In our study, Bn and CD27<sup>-</sup> Sw Bm significantly and positively correlated with better survival, whereas PCs, IgM<sup>+</sup> Bm, and CD27<sup>+</sup> Sw Bm have not demonstrated independently prognostic values. Thus, it is highly possible that Bn and CD27<sup>-</sup> Sw Bm may play the predominant role in the prognostic effect of B cells. In fact, Bn could express CD80, CD86, CXCR3, CCR5,<sup>32</sup> and PD1,<sup>33</sup> indicating that Bn may help T cell activation. In addition, CD27<sup>-</sup> Sw Bm were capable of produce IgG or IgA to promote humoral immunity.<sup>34,35</sup> Considering that PCs, IgM<sup>+</sup> Bm, and CD27<sup>+</sup> Sw Bm have no prognostic value, we assumed that certain unknown subsets within them may have lost anti-tumor activity, or even shift toward the tumor-promoting direction.

For example, using four markers CD20<sup>-</sup>CD24<sup>-</sup>CD27<sup>hi</sup>CD38<sup>hi</sup> to define PCs, we found that, although PCs were the most abundant component within total B cells in tumor tissues, PCs had no prognostic value in the validation cohort. In contrast, a recent study reported that PCs, defined as CD20<sup>-</sup>CD79 $\alpha$ <sup>+</sup> cells, were significantly associated with better prognosis in HCC.<sup>36</sup> PCs

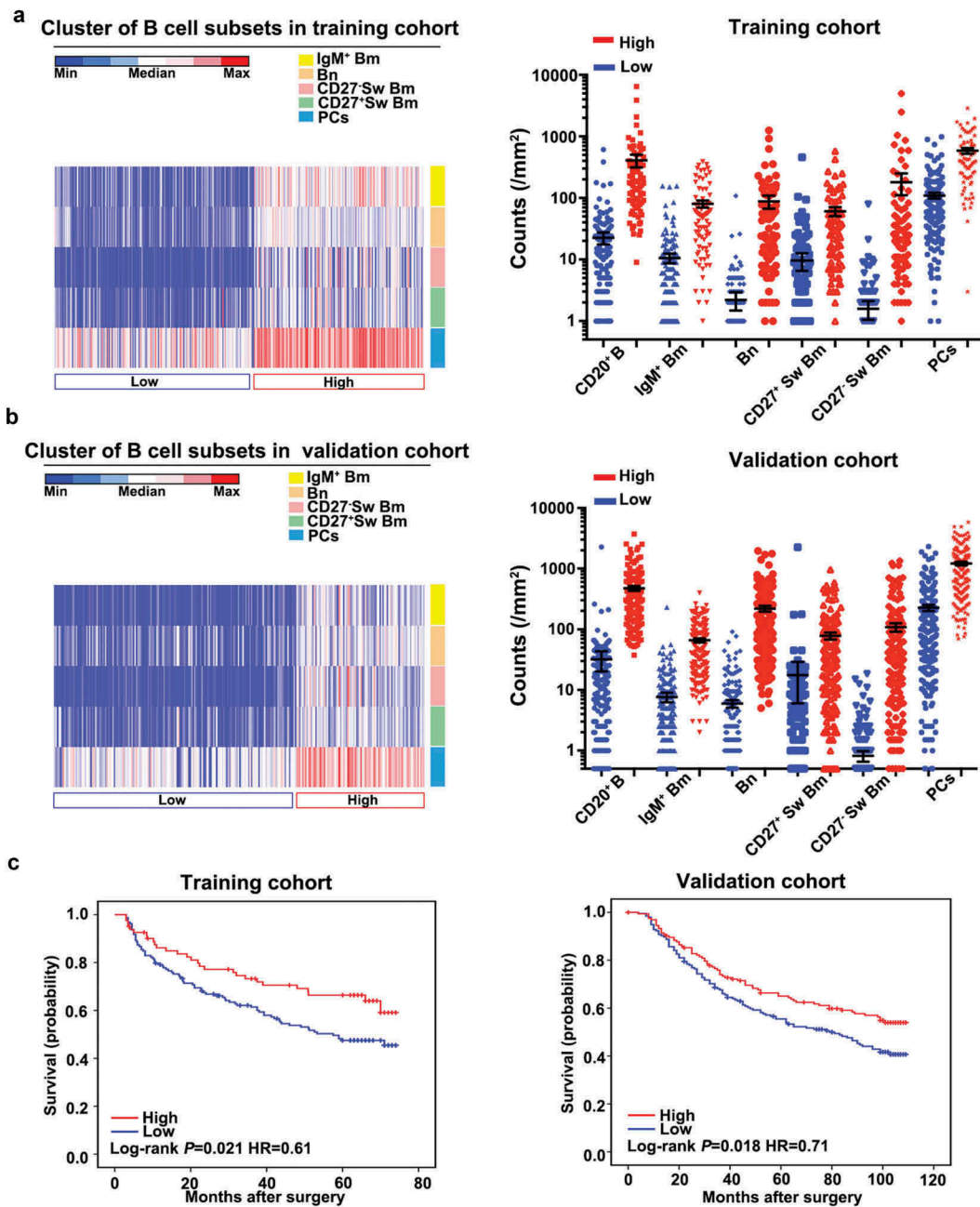


**Figure 5.** Cluster analysis based on B cell density enables patient classification in HCC. (a and b) Heat maps described the result of unsupervised cluster analysis according to densities of B cell subsets in tumor tissues from two independent cohorts. (c) Kaplan-Meier analysis of OS stratified by clustering analysis in the training and validation cohorts.

were considered to be producers of antibodies, secreting IgA, IgG, and IgM. They can also serve as APC and express some costimulatory molecules, including CD80 and CD86.<sup>37</sup> However, some studies provide evidence that the regulatory PCs had the ability to inhibit T cell response by producing IL-10<sup>38</sup> and IL-35.<sup>39</sup> Therefore, it is tempting to suggest both pro-tumorigenic and anti-tumorigenic subsets of PCs may exist in human cancer, including HCC. For instance, increased intratumoral PCs, defined as CD138<sup>+</sup> cells were associated with reduced survival in ovarian cancer,<sup>40</sup> but correlated with improved outcome in the lung,<sup>41</sup> ovarian,<sup>42</sup> and esophagogastric cancers.<sup>43</sup> Further investigation on the precise function and repertoire feature of each B cell subset

or subpopulations within given subset by advanced techniques, such as the single-cell method, is needed.

In summary, our study not only shows the technical advance of multiplexed immunohistochemistry to “see” B cell subsets *in situ* and reveals the complex B cell subsets within HCC but also opens new opportunities to perform an in-depth study in the near future. Further investigation of the specific composition and functions of B cell subsets will help us to better understand their roles in HCC. Immunotherapies aiming at selectively depleting the pro-tumorigenic B cell subsets and/or expanding the anti-tumorigenic subsets will clearly provide the new opportunities for HCC therapies.



## Materials and methods

### Patients and specimens

Two independent cohorts of HCC patients (training cohort:  $n = 258$ ; validation cohort:  $n = 361$ ) receiving curative resection at Zhongshan Hospital of Fudan University in 2006 and 2007, respectively, were retrospectively reviewed and enrolled in this study. Detailed clinicopathologic characteristics are summarized in Supplementary Table S7. No significant differences in clinicopathologic characteristics were found between these two cohorts. Informed consent was signed by each patient, and ethical approval was obtained from the Zhongshan Hospital Research Ethics Committee.

### Tissue microarray

Tissue microarrays were constructed as described previously.<sup>44</sup> Briefly, all HCC cases were reviewed histologically using hematoxylin and eosin staining. Duplicates from two different areas, as intratumor tissues and paired non-tumor liver tissues, were obtained in each case. Finally, two independent cohorts of TMA were constructed (Shanghai Biochip CoLtd, Shanghai, China). Sections of 4  $\mu\text{m}$  thick were placed on slides coated with 3-aminopropyltriethoxysilane.

### Multiplexed immunohistochemistry staining

Before multiplexed staining, antibody validation was performed using tonsil and spleen as positive controls and on HCC tissues (Supplementary Figure S1A). Multiplexed immunohistochemistry staining was carried out according to the manufacturer's instructions as described previously.<sup>45</sup> The process was conducted for the following antibodies/fluorescent dyes, in order: CD24/opal 570, CD38/opal 690, IgM/opal 620, CD20/opal 520, CD27/opal 650 (Supplementary Table S8). Detailed procedures of multiplexed staining are provided in Supplemental Materials and Methods.

### Multispectral imaging and analysis

Multiplex stained TMA slides were scanned using the Vectra 3 automated, high-throughput multiplexed biomarker imaging system (Perkin Elmer). Cells were classified into the following types: plasma cells (PCs) ( $\text{CD}20^- \text{CD}24^- \text{CD}27^{\text{hi}} \text{CD}38^{\text{hi}}$ ), B cells ( $\text{CD}20^+$ ), naive B cells (Bn) ( $\text{CD}20^+ \text{CD}27^- \text{IgM}^+$ ),  $\text{IgM}^+$  memory B cells ( $\text{IgM}^+ \text{Bm}$ ) ( $\text{CD}20^+ \text{CD}27^+ \text{IgM}^+$ ),  $\text{CD}27^-$  isotype-switched memory B cells ( $\text{CD}27^- \text{Sw Bm}$ ) ( $\text{CD}20^+ \text{CD}27^- \text{IgM}^-$ ), and  $\text{CD}27^+$  isotype-switched memory B cells ( $\text{CD}27^+ \text{Sw Bm}$ ) ( $\text{CD}20^+ \text{CD}27^+ \text{IgM}^-$ ). All pixel intensity information was filed into image cytometry data analysis software, FCS Express 6 Plus v6.04.0034 (De Novo Software). Detailed procedures of multiplexed imaging are provided in Supplemental Materials and Methods.

### Dimension reduction analysis and clustering analysis

We first chose the cells belonging to five distinct groups (Bn,  $\text{IgM}^+ \text{Bm}$ ,  $\text{CD}27^- \text{Sw Bm}$ ,  $\text{CD}27^+ \text{Sw Bm}$ , and PCs). Then 1000 cells from each group were chosen to form an  $n \times 5$  matrix (where  $n$  is the number of cells used,  $n = 1000$ , and 5 is feature number including Cytoplasm CD20, Cytoplasm CD24, Cytoplasm IgM, Cytoplasm CD27, and Cytoplasm CD38). Then the dimension of data was subsequently reduced to 2 using the t-SNE technique<sup>46</sup> (Matlab code obtained from <https://lvdmaaten.github.io/tsne/was> used and the low dimensional points generated preserve pairwise similarity of the original data set). Finally, the low-dimensional points were coded by the groups as shown. For clustering, an unsupervised clustering analysis was performed with the k-means clustering analysis (Built-in Matlab function was used). The Euclidean distance was used in k-means clustering.

### Flow cytometry analysis

Flow cytometry was used to detect the surface markers of B cells isolated from 10 patients with HCC. Peripheral blood mononuclear cells (PBMC) were isolated by ficoll density gradient centrifugation based on the manufacturer's protocols. Single cell suspensions from fresh paired tumor tissues and non-tumor tissues were obtained by tissue digestion as described previously.<sup>25</sup> Surface markers were used to separate the B cell subsets as follows: CD3, CD20, CD24, CD27, CD38, IgM, and IgD (Supplementary Table S7). After gating out  $\text{CD}3^+$  T cells, cells were gated into  $\text{CD}20^+$  B cells and  $\text{CD}20^-$  fraction.  $\text{CD}20^+$  B cells were further divided into Bn ( $\text{CD}20^+ \text{IgM}^+ \text{IgD}^+ \text{CD}27^-$ ),  $\text{IgM}^+ \text{Bm}$  ( $\text{CD}20^+ \text{IgM}^+ \text{IgD}^+ \text{CD}27^+$ ),  $\text{CD}27^+ \text{Sw Bm}$  ( $\text{CD}20^+ \text{IgM}^- \text{IgD}^- \text{CD}27^+$ ),  $\text{CD}27^- \text{Sw Bm}$  ( $\text{CD}20^+ \text{IgM}^- \text{IgD}^- \text{CD}27^-$ ). PCs were defined from  $\text{CD}20^-$  fraction as  $\text{CD}20^- \text{CD}27^{\text{hi}} \text{CD}38^{\text{hi}}$ . Flow cytometry was performed on a BD LSR Fortessa cell analyzer (BD Bioscience) according to the manufacturer's instructions and analyzed by FlowJo software version 9.3.2.

More details are provided in Supplemental Materials and Methods.

### Statistical analyses

Statistical analyses were performed using SPSS 22 software (IBM, Armonk, NY, USA), and Graph Pad Prism 6.0 (Graph Pad Soft Inc, San Diego, CA, USA). The relationship of variables was analyzed by a two-tailed Student's t-test, Pearson's correlation test, Pearson chi-square test or Chi-square with Yates' correction when appropriate. Multivariate analyses were based on the Cox proportional hazards regression model. Receiver operating characteristic curve (ROC) was used to determine the optimal cut off value. Accordingly, patients were stratified in to low and high groups. Then, Kaplan-Meier analysis (log-rank test) was used to describe differences in patients' overall survival (OS). A two-tailed  $P$  value  $< 0.05$  was considered statistically significant.

## Additional information

### Ethics approval

This study confirmed strictly to the ethical guidelines of the Declaration of Helsinki and was approved by the Zhongshan Hospital Research Ethics Committee.

### Informed consent

Informed consent was obtained from all individual participants included in the study.

### Disclosure of Potential Conflicts of Interest

The authors declare no potential conflict of interest.

### Funding

This work was supported by the Strategic Priority Research Program (No. XDB29030302), Interdisciplinary Innovation Team, Frontier Science Key Research Project (No. QYZDB-SSW-SMC036), Chinese Academy of Sciences; National Key Basic Research Program of China (Nos. 2014CB541904, 2015CB856000) and the National Natural Science Foundation of China (Nos. 31270961, 31470879, 81861138010, 81522036, 81872321, and 81802302).

### Abbreviations

|                     |                                    |
|---------------------|------------------------------------|
| HCC                 | hepatocellular carcinoma           |
| TME                 | tumor microenvironment             |
| PD-1                | programmed cell death protein-1    |
| IL-10               | interleukin-10                     |
| IL-35               | interleukin-35                     |
| IFN- $\gamma$       | interferon- $\gamma$               |
| TMA                 | tissue microarrays                 |
| TSA                 | tyramide signal amplification      |
| OS                  | overall survival                   |
| HR                  | hazard ratio                       |
| TNM                 | tumor node metastasis              |
| DAB                 | 3,3'-diaminobenzidine              |
| PBMC                | peripheral blood mononuclear cells |
| Bn                  | naive B cells                      |
| IgM <sup>+</sup> Bm | IgM <sup>+</sup> memory B cells    |
| Sw Bm               | isotype-switched memory B cells    |
| PCs                 | plasma cells                       |
| TCGA                | The Cancer Genome Atlas            |

### References

- European Association for the Study of the Liver. EASL clinical practice guidelines: management of hepatocellular carcinoma. *J Hepatol.* 2018;69:182–236. doi:10.1016/j.jhep.2018.03.019.
- Chen CJ. Global elimination of viral hepatitis and hepatocellular carcinoma: opportunities and challenges. *Gut.* 2018;67:595–598. doi:10.1136/gutjnl-2017-315407.
- Ray K. Liver cancer: a complex interplay between inflammation and immunity in liver cancer. *Nat Rev Gastroenterol Hepatol.* 2018;15:3. doi:10.1038/nrgastro.2017.165.
- El-Khoueiry AB, Sangro B, Yau T, Crocenzi TS, Kudo M, Hsu C, Kim T.Y., Choo S.P., Trojan J., Welling T.H. 3rd, et al. Nivolumab in patients with advanced hepatocellular carcinoma (CheckMate 040): an open-label, non-comparative, phase 1/2 dose escalation and expansion trial. *Lancet.* 2017;389:2492–2502. doi:10.1016/S0140-6736(17)31046-2.
- Ringelhan M, Pfister D, O'Connor T, Pikarsky E, Heikenwalder M. The immunology of hepatocellular carcinoma. *Nat Immunol.* 2018;19:222–232. doi:10.1038/s41590-018-0044-z.
- Zheng C, Zheng L, Yoo JK, Guo H, Zhang Y, Guo X, Kang B., Hu R., Huang J.Y., Zhang Q., et al. Landscape of infiltrating T cells in liver cancer revealed by single-cell sequencing. *Cell.* 2017;169:1342–56 e16. doi:10.1016/j.cell.2017.05.035.
- Brown CE, Alizadeh D, Starr R, Weng L, Wagner JR, Naranjo A, Ostberg J.R., Blanchard, M.S., Kilpatrick J., Simpson J., et al. Regression of glioblastoma after chimeric antigen receptor T-cell therapy. *N Engl J Med.* 2016;375:2561–2569. doi:10.1056/NEJMoa1610497.
- Gitlin AD, Nussenzweig MC. Immunology: fifty years of B lymphocytes. *Nature.* 2015;517:139–141. doi:10.1038/517139a.
- Cooper MD. The early history of B cells. *Nat Rev Immunol.* 2015;15:191–197. doi:10.1038/nri3801.
- Shen M, Wang J, Yu W, Zhang C, Liu M, Wang K, Yang, L., Wei F., Wang S.E., Sun Q., et al. A novel MDSC-induced PD-1(–) PD-L1(+) B-cell subset in breast tumor microenvironment possesses immuno-suppressive properties. *Oncoimmunology.* 2018;7:e1413520. doi:10.1080/2162402X.2018.1490854.
- Taghavi N, Mohsenifar Z, Baghban AA, Arjomandkhan A. CD20 + tumor infiltrating b lymphocyte in oral squamous cell carcinoma: correlation with clinicopathologic characteristics and heat shock protein 70 expression. *Patholog Res Int.* 2018;2018:4810751. doi:10.1155/2018/4810751.
- Germain C, Gnjatich S, Tamzalit F, Knockaert S, Remark R, Goc J, Lepelley A., Becht E., Katsahian S., Bizouard, G., et al. Presence of B cells in tertiary lymphoid structures is associated with a protective immunity in patients with lung cancer. *Am J Respir Crit Care Med.* 2014;189:832–844. doi:10.1164/rccm.201309-1611OC.
- Al-Shibli KI, Donnem T, Al-Saad S, Persson M, Bremnes RM, Busund LT. Prognostic effect of epithelial and stromal lymphocyte infiltration in non-small cell lung cancer. *Clin Cancer Res.* 2008;14:5220–5227. doi:10.1158/1078-0432.CCR-08-0133.
- Nielsen JS, Sahota RA, Milne K, Kost SE, Nesslinger NJ, Watson PH, Nelson B.H. CD20+ tumor-infiltrating lymphocytes have an atypical CD27- memory phenotype and together with CD8+ T cells promote favorable prognosis in ovarian cancer. *Clin Cancer Res.* 2012;18:3281–3292. doi:10.1158/1078-0432.CCR-12-0234.
- Erdag G, Schaefer JT, Smolkin ME, Deacon DH, Shea SM, Dengel LT, Patterson JW, Slingsluff CL. Immunotype and immunohistologic characteristics of tumor-infiltrating immune cells are associated with clinical outcome in metastatic melanoma. *Cancer Res.* 2012;72:1070–1080. doi:10.1158/0008-5472.CAN-11-3218.
- Linnebacher M, Maletzki C. Tumor-infiltrating B cells: the ignored players in tumor immunology. *Oncoimmunology.* 2012;1:1186–1188. doi:10.4161/onci.20641.
- Yuen GJ, Demissie E, Pillai S. B lymphocytes and cancer: a love-hate relationship. *Trends Cancer.* 2016;2:747–757. doi:10.1016/j.trecan.2016.10.010.
- Chapoval AI, Fuller JA, Kremlev SG, Kamdar SJ, Evans R. Combination chemotherapy and IL-15 administration induce permanent tumor regression in a mouse lung tumor model: NK and T cell-mediated effects antagonized by B cells. *J Immunol.* 1990;149:6977–6984.
- Woo JR, Liss MA, Muldong MT, Palazzi K, Strasner A, Ammirante M, Varki N., Shabaik A., Howell S., Kane C.J., et al. Tumor infiltrating B-cells are increased in prostate cancer tissue. *J Transl Med.* 2014;12:30. doi:10.1186/1479-5876-12-30.
- Ammirante M, Luo JL, Grivennikov S, Nedospasov S, Karin M. B-cell-derived lymphotoxin promotes castration-resistant prostate cancer. *Nature.* 2010;464:302–305. doi:10.1038/nature08782.
- Staquicini FI, Tandle A, Libutti SK, Sun J, Zigler M, Bar-Eli M, Aliperti F, Pérez EC, Gershenwald JE, Mariano M, et al. A subset of host B lymphocytes controls melanoma metastasis through a melanoma cell adhesion molecule/MUC18-dependent interaction: evidence from mice and humans. *Cancer Res.* 2008;68:8419–8428. doi:10.1158/0008-5472.CAN-08-1242.

22. Somasundaram R, Zhang G, Fukunaga-Kalabis M, Perego M, Krepler C, Xu X, Wagner C., Hristova D., Zhang J., Tian T., et al. Tumor-associated B-cells induce tumor heterogeneity and therapy resistance. *Nat Commun.* 2017;8:607. doi:10.1038/s41467-017-00452-4.
23. Pylyayeva-Gupta Y, Das S, Handler JS, Hajdu CH, Coffre M, Korolov SB, Bar-Sagi D. IL35-producing B cells promote the development of pancreatic neoplasia. *Cancer Discov.* 2016;6:247–255. doi:10.1158/2159-8290.CD-15-0843.
24. de Visser KE, Korets LV, Coussens LM. De novo carcinogenesis promoted by chronic inflammation is B lymphocyte dependent. *Cancer Cell.* 2005;7:411–423. doi:10.1016/j.ccr.2005.04.014.
25. Shi JY, Gao Q, Wang ZC, Zhou J, Wang XY, Min ZH, Shi Y-H, Shi G-M, Ding Z-B, Ke A-W, et al. Margin-infiltrating CD20(+) B cells display an atypical memory phenotype and correlate with favorable prognosis in hepatocellular carcinoma. *Clin Cancer Res.* 2013;19:5994–6005. doi:10.1158/1078-0432.CCR-12-3497.
26. Xiao X, Lao XM, Chen MM, Liu RX, Wei Y, Ouyang FZ, Chen D. P., Zhao X.Y., Zhao Q., Li X.F. et al. PD-1hi identifies a novel regulatory B-cell population in human hepatoma that promotes disease progression. *Cancer Discov.* 2016;6:546–559. doi:10.1158/2159-8290.CD-15-1408.
27. Liu RX, Wei Y, Zeng QH, Chan KW, Xiao X, Zhao XY, Ouyang F. Z., Chen D.P., Zheng L., Lao X.M. Chemokine (C-X-C motif) receptor 3-positive B cells link interleukin-17 inflammation to protumorigenic macrophage polarization in human hepatocellular carcinoma. *Hepatology.* 2015;62:1779–1790. doi:10.1002/hep.28020.
28. Deenick EK, Avery DT, Chan A, Berglund LJ, Ives ML, Moens L, Stoddard J.L., Bustamante J., Boisson-Dupuis S., Tsumura M., et al. Naive and memory human B cells have distinct requirements for STAT3 activation to differentiate into antibody-secreting plasma cells. *J Exp Med.* 2013;210:2739–2753. doi:10.1084/jem.20130323.
29. Seifert M, Przekopowicz M, Taudien S, Lollies A, Ronge V, Drees B, Lindemann M., Hillen U., Engler H., Singer B.B., et al. Functional capacities of human IgM memory B cells in early inflammatory responses and secondary germinal center reactions. *Proc Natl Acad Sci USA.* 2015;112:E546–55. doi:10.1073/pnas.1416276112.
30. Faggioli F, Palagano E, Di Tommaso L, Donadon M, Marrella V, Recordati C, Mantero S., Villa, A., Vezzoni P., Cassani B. B lymphocytes limit senescence-driven fibrosis resolution and favor hepatocarcinogenesis in mouse liver injury. *Hepatology.* 2018;67:1970–1985. doi:10.1002/hep.29636.
31. Ouyang FZ, Wu RQ, Wei Y, Liu RX, Yang D, Xiao X, Zheng L., Li B., Lao XM., et al. Dendritic cell-elicited B-cell activation fosters immune privilege via IL-10 signals in hepatocellular carcinoma. *Nat Commun.* 2016;7:13453. doi:10.1038/ncomms13453.
32. Niino M, Hirotani M, Miyazaki Y, Sasaki H. Memory and naive B-cell subsets in patients with multiple sclerosis. *Neurosci Lett.* 2009;464:74–78. doi:10.1016/j.neulet.2009.08.010.
33. Thibault ML, Mamessier E, Gertner-Dardenne J, Pastor S, Just-Landi S, Xerri L, Chetaille B, Olive D. PD-1 is a novel regulator of human B-cell activation. *Int Immunol.* 2013;25:129–137. doi:10.1093/intimm/dxs098.
34. Fecteau JF, Cote G, Neron S. A new memory CD27-IgG+ B cell population in peripheral blood expressing VH genes with low frequency of somatic mutation. *J Immunol.* 2006;177:3728–3736.
35. Berkowska MA, Schickel JN, Grosse-Heiter-Wagener C, de Ridder D, Ng YS, van Dongen JJ, Meffre E., Van Zelm, M.C. Circulating human CD27-IgA+ memory B cells recognize bacteria with polyreactive Igs. *J Immunol.* 1950;2015(195):1417–1426.
36. Kurebayashi Y, Ojima H, Tsujikawa H, Kubota N, Maehara J, Abe Y, Kitago, M., Shinoda, M., Kitagawa, Y., Sakamoto, M. Landscape of immune microenvironment in hepatocellular carcinoma and its additional impact on histological and molecular classification. *Hepatology.* 2018. doi:10.1002/hep.29904.
37. Tiburzy B, Kulkarni U, Hauser AE, Abram M, Manz RA. Plasma cells in immunopathology: concepts and therapeutic strategies. *Semin Immunopathol.* 2014;36:277–288. doi:10.1007/s00281-014-0426-8.
38. Neves P, Lampropoulou V, Calderon-Gomez E, Roch T, Stervbo U, Shen P, Kühl A.A., Loddenkemper C., Haury M., Nedospasov S.A., et al. Signaling via the MyD88 adaptor protein in B cells suppresses protective immunity during Salmonella typhimurium infection. *Immunity.* 2010;33:777–790. doi:10.1016/j.immuni.2010.10.016.
39. Shen P, Roch T, Lampropoulou V, O'Connor RA, Stervbo U, Hilgenberg E, Ries S., Jaimes Y., Daridon C., Li R., et al. IL-35-producing B cells are critical regulators of immunity during autoimmune and infectious diseases. *Nature.* 2014;507:366–370. doi:10.1038/nature12979.
40. Lundgren S, Berntsson J, Nodin B, Micke P, Jirstrom K. Prognostic impact of tumour-associated B cells and plasma cells in epithelial ovarian cancer. *J Ovarian Res.* 2016;9:21. doi:10.1186/s13048-016-0232-0.
41. Lohr M, Edlund K, Botling J, Hammad S, Hellwig B, Othman A, Berglund, A., Lambe, M., Holmberg, L., Ekman, S., et al. The prognostic relevance of tumour-infiltrating plasma cells and immunoglobulin kappa C indicates an important role of the humoral immune response in non-small cell lung cancer. *Cancer Lett.* 2013;333:222–228. doi:10.1016/j.canlet.2013.01.036.
42. Kroeger DR, Milne K, Nelson BH. Tumor-infiltrating plasma cells are associated with tertiary lymphoid structures, cytolytic T-cell responses, and superior prognosis in ovarian cancer. *Clin Cancer Res.* 2016;22:3005–3015. doi:10.1158/1078-0432.CCR-15-2762.
43. Knief J, Reddemann K, Petrova E, Herhahn T, Wellner U, Thorns C. High density of tumor-infiltrating B-lymphocytes and plasma cells signifies prolonged overall survival in adenocarcinoma of the esophagogastric junction. *Anticancer Res.* 2016;36:5339–5345. doi:10.21873/anticancer.11107.
44. Gao Q, Qiu SJ, Fan J, Zhou J, Wang XY, Xiao YS, Xu Y, Li Y-W, Tang Z-Y. Intratumoral balance of regulatory and cytotoxic T cells is associated with prognosis of hepatocellular carcinoma after resection. *J Clin Oncol.* 2007;25:2586–2593. doi:10.1200/JCO.2006.09.4565.
45. Stack EC, Wang C, Roman KA, Hoyt CC. Multiplexed immunohistochemistry, imaging, and quantitation: a review, with an assessment of tyramide signal amplification, multispectral imaging and multiplex analysis. *Methods.* 2014;70:46–58. doi:10.1016/j.jymeth.2014.08.016.
46. van der Maaten L, Hinton G. Visualizing data using t-SNE. *J Mach Learn Res.* 2008;9:2579–2605.